LETTERS
PUBLISHED ONLINE: 7 DECEMBER 2015 | DOI: 10.1038/NPHYS3580
nature physics

Superconductivity protected by spin–valley locking in ion-gated MoS_2

Yu Saito[1]*, Yasuharu Nakamura[2,3], Mohammad Saeed Bahramy[1,4], Yoshimitsu Kohama[5], Jianting Ye[1,4], Yuichi Kasahara[3], Yuji Nakagawa[1], Masaru Onga[1], Masashi Tokunaga[5], Tsutomu Nojima[6], Youichi Yanase[3,7] and Yoshihiro Iwasa[1,4]*

Symmetry-breaking has been known to play a key role in non-centrosymmetric superconductors with strong spin–orbit interactions (SOIs; refs 1–6). The studies, however, have been so far mainly focused on a particular type of SOI, known as the Rashba SOI (ref. 7), whereby the electron spin is locked to its momentum at a right-angle, thereby leading to an in-plane helical spin texture. Here we discuss electric-field-induced superconductivity in molybdenum disulphide (MoS_2), which exhibits a fundamentally different type of intrinsic SOI, manifested by an out-of-plane Zeeman-type spin polarization of energy valleys[8–10]. We find an upper critical field of approximately 52 T at 1.5 K, which indicates an enhancement of the Pauli limit by a factor of four as compared to that in centrosymmetric conventional superconductors. Using realistic tight-binding calculations, we reveal that this unusual behaviour is due to an inter-valley pairing that is symmetrically protected by Zeeman-type spin–valley locking against external magnetic fields. Our study sheds light on the interplay of inversion asymmetry with SOIs in confined geometries, and its role in superconductivity.

MoS_2 is a member of the layered semiconducting transition metal dichalcogenides (TMDs; ref. 11), which have been attracting widespread attention as two-dimensional (2D) materials beyond graphene, owing to their multiple functionalities with potential applications such as atomically thin electronics[12–14], photonics[15] and valleytronics devices utilizing a coupled spin and valley degree of freedom[16–18]. Also, MoS_2 is becoming a new platform for investigating quantum physics—for example, with quantum oscillations[19] and electric-field-induced superconductivity[20]. The unit cell of MoS_2 is composed of two formula units, in each of which one Mo atom is sandwiched between two S atoms, forming a S–Mo–S monolayer stacking along the c-axis with D_{3h} symmetry (Fig. 1a). In the isolated monolayer, in-plane inversion symmetry is broken, causing out-of-plane spin polarization together with effective Zeeman fields—namely, Zeeman-type spin polarization at zero magnetic field[8–10,21]. This Zeeman-type spin splitting reaches 3 meV (ref. 22) and 148 meV (ref. 8) at the bottom of conduction band and the top of the valence band, respectively, both of which are located at the K points, the corner of the hexagonal first Brillouin zone shown in Fig. 1b. Such a zero-field spin splitting is not observed in bulk MoS_2 with D^4_{6h} symmetry[23,24]. Also, this spin splitting changes its sign at the −K point, because the K and −K points are connected by the time-reversal operation. Such a spin splitting unique to monolayer MoS_2 originates from the fairly strong SOI of transition metal d-orbitals, and is commonly observed in the group VI of TMD semiconductors[8,9]. This valley-dependent spin polarization is in marked contrast to the in-plane momentum-dependent spin polarization caused by the Rashba-type SOI (ref. 7).

A non-centrosymmetric system with considerable SOIs is an ideal platform for exotic superconductivity—in fact, superconductivity occurring in the Rashba-type band structure has been intensively investigated on a variety of systems[1–4], together with the effect of spin–momentum locking. However, the effect of Zeeman-type spin polarization on superconductivity has not been discussed previously. Here, we investigate electric-field-induced superconductivity in MoS_2 by using an electric-double-layer transistor (EDLT) configuration (Fig. 1c), which creates a high-density two-dimensional electron system (2DES) on the surface (Fig. 1d) without introducing extrinsic disorder, thereby offering novel opportunities to search for new types of exotic superconductivity[25–27].

To extract the anomalous features of electric-field-induced superconductivity at the highly crystalline multilayer MoS_2 surface, we fabricated an EDLT structure with a 20-nm-thick flake, and then performed magneto-transport measurements. The MoS_2-EDLT underwent a superconducting transition at a gate voltage of $V_G = 6.5$ V and a sheet carrier density of $n_{2D} = 1.5 \times 10^{14}$ cm^{-2} measured at 15 K (Fig. 2a). The critical temperature, T_c, of this device was 9.7 K, as defined at the midpoint of the transition, with R_{sheet} being 50% of the normal state sheet resistance at 15 K. This carrier density is slightly larger than the optimum value in the dome-shaped phase diagram[20,28,29]. The electrochemical reaction is unlikely even at high gate voltages up to 6.5 V (see Supplementary Section I), according to the reversibility and the absence of hysteresis in the transfer curve (Supplementary Fig. 1). Zoom-ins to the resistive transition in the low-temperature region under the application of perpendicular and parallel magnetic fields from 0 to 9 T are shown in Fig. 2b and c, respectively. The superconducting state is completely quenched at 9 T for perpendicular magnetic fields (Fig. 2b), whereas it remains almost unchanged in the in-plane magnetic field geometry (Fig. 2c). This behaviour indicates a substantially large anisotropy in the superconductivity. Figure 2d shows the angular dependence of the upper critical field, $H_{c2}(\theta)$, at 9.6 K (θ represents the angle between the c-axis of the crystal

[1]Quantum-Phase Electronics Center (QPEC) and Department of Applied Physics, The University of Tokyo, Tokyo 113-8656, Japan. [2]Graduate School of Science and Technology, Niigata University, Niigata 950-2181, Japan. [3]Department of Physics, Kyoto University, Kyoto 606-8502, Japan. [4]RIKEN Center for Emergent Matter Science (CEMS), Wako 351-0198, Japan. [5]International MegaGauss Science Laboratory, Institute for Solid State Physics, The University of Tokyo, Kashiwa 277-8581, Japan. [6]Institute for Materials Research, Tohoku University, Sendai 980-8577, Japan. [7]Department of Physics, Niigata University, Niigata 950-2181, Japan. *e-mail: saito@mp.t.u-tokyo.ac.jp; iwasa@ap.t.u-tokyo.ac.jp

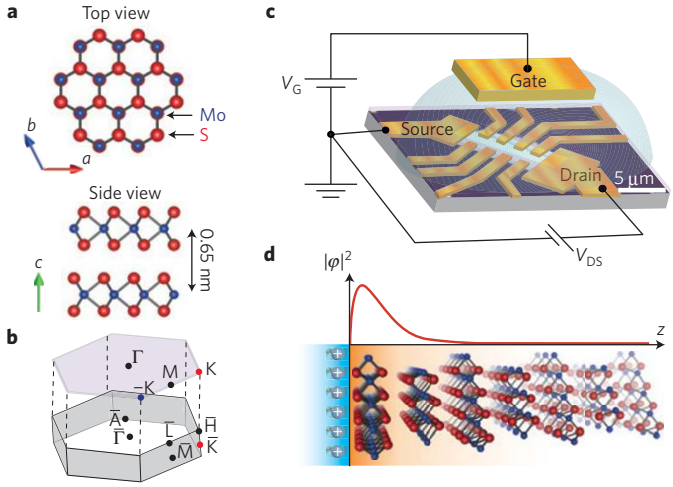

Figure 1 | Crystal structure of MoS_2 and conceptual images of a MoS_2-EDLT. a, Ball-and-stick model of the bulk crystal structure of MoS_2 in top and side views. **b**, Corresponding bulk (bottom) and monolayer (top) Brillouin zone. **c**, Schematic image of the MoS_2-EDLT. **d**, Schematic interface carrier profile in the MoS_2-EDLT.

and the direction of the applied magnetic fields). Here, $H_{c2}(\theta)$ is also determined by the midpoint of the resistive transition. A cusp-like peak in the inset of Fig. 2d is described well by the 2D Tinkham model[30] (and not by the 3D anisotropic mass model) as frequently observed in interfacial superconductivity[31–33]. In addition, the dependence of H_{c2} on the temperature T for both the out-of-plane and in-plane magnetic fields (Fig. 2e) are fitted well by the phenomenological 2D Ginzburg–Landau (GL) model,

$$\mu_0 H_{c2}^{\perp} = \frac{\Phi_0}{2\pi\xi_{GL}(0)^2}(1 - T/T_c)$$

and

$$\mu_0 H_{c2}^{\parallel} = \frac{\Phi_0\sqrt{12}}{2\pi\xi_{GL}(0)d_{SC}}\sqrt{1 - T/T_c}$$

where Φ_0, $\xi_{GL}(0)$ and d_{SC} denote a flux quantum, the in-plane GL coherence length at $T = 0$ K, and the effective thickness of superconductivity, respectively. We find $\xi_{GL}(0) = 8.0$ nm and $d_{SC} = 1.5$ nm. Note that the extremely sharp rise of $H_{c2}^{\parallel}(T)$ near T_c shows a marked contrast to that in conventional bulk layered superconductors such as Cs-doped MoS_2 (ref. 34), demonstrating that the present system is extremely 2D in nature. In fact, $H_{c2}^{\parallel}(T)$ can seemingly go far beyond the Pauli limit, H_P^{BCS}, for weak coupling Bardeen–Cooper–Schrieffer (BCS) superconductors, $\mu_0 H_P^{BCS} = \Delta_0/\sqrt{2}k_B T_c = 1.86 T_c = 18$ T, where k_B and Δ_0 are the Boltzmann constant and the BCS-theory-based superconducting gap at $T = 0$ K, respectively.

To investigate $H_{c2}^{\parallel}$ at much lower temperatures, we measured the magnetoresistance of another MoS_2-EDLT by applying pulsed magnetic fields up to 55 T (see Supplementary Section II and Supplementary Fig. 2). A clear resistance drop at a T_c of 6.5 K was observed, which was defined as the temperature where R_{sheet} reached 75% of the normal state sheet resistance, indicating a superconducting signature, although the MoS_2-EDLT used for the measurements in high magnetic fields ($n_{2D} = 8.5 \times 10^{13}$ cm^{-2} at $V_G = 5.5$ V and $T = 15$ K) did not exhibit zero resistance. The magnetoresistance of the MoS_2-EDLT is shown in Fig. 3a and b for out-of-plane and in-plane magnetic fields, respectively, at several temperatures between 1.5 and 8.0 K. In the out-of-plane magnetic field geometry, the superconducting state is completely destroyed

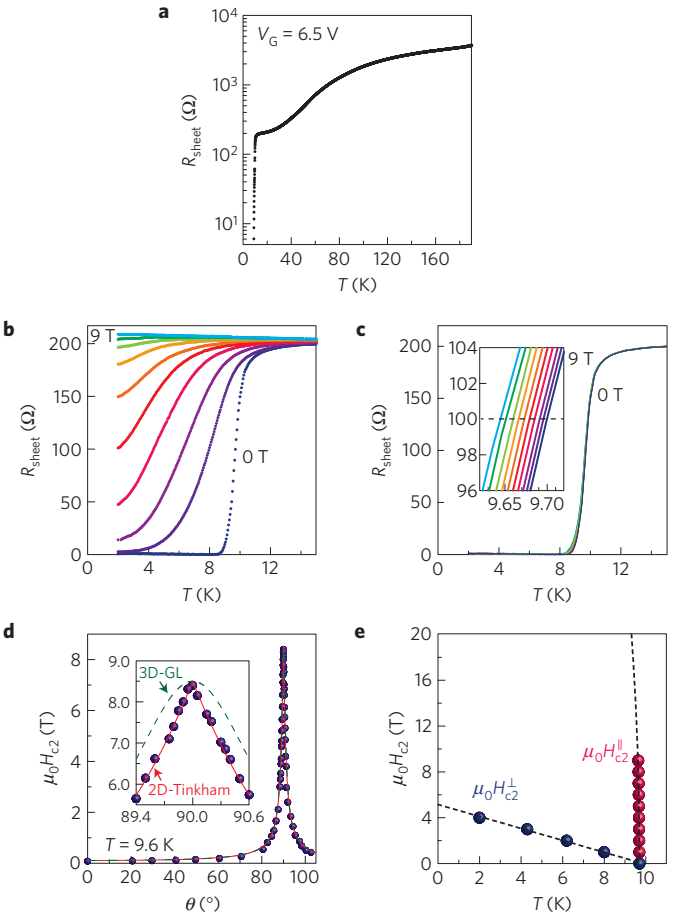

Figure 2 | Two-dimensional superconductivity in ion-gated MoS_2. a, Sheet resistance as a function of temperature at $V_G = 6.5$ V. The superconducting transition was observed at $T = 9.7$ K and $\mu_0 H = 0$ T. **b**,**c**, Sheet resistance of a MoS_2-EDLT as a function of temperature at $V_G = 6.5$ V, for perpendicular magnetic fields, $\mu_0 H_{c2}^{\perp}$ (**b**), and parallel magnetic fields, $\mu_0 H_{c2}^{\parallel}$ (**c**), varying in 1 T steps from 0 to 9 T. The inset of **c** shows a close-up of the resistive transition near the midpoint of the normal state sheet resistance (black dashed line). **d**, Angular dependence of the upper critical field, $\mu_0 H_{c2}(\theta)$, where θ is the angle between the magnetic field and the direction perpendicular to the surface of MoS_2). The inset shows a magnified view of the region around $\theta = 90°$. For the theoretical representation of $H_{c2}(\theta)$ the red solid line corresponds to the 2D Tinkham's formula $((H_{c2}(\theta)\sin\theta)/H_{c2}^{\parallel})^2 + |(H_{c2}(\theta)\cos\theta)/H_{c2}^{\perp}| = 1$ and the green dashed line corresponds to the 3D anisotropic mass model (3D-GL) $((H_{c2}(\theta)\sin\theta)/H_{c2}^{\parallel})^2 + ((H_{c2}(\theta)\cos\theta)/H_{c2}^{\perp})^2 = 1$. **e**, Temperature dependence of $\mu_0 H_{c2}$ perpendicular and parallel to the surface, $\mu_0 H_{c2}^{\perp}(T)$ and $\mu_0 H_{c2}^{\parallel}(T)$. Black dashed curves indicate the theoretical values obtained from the 2D-GL equations.

by the application of magnetic fields stronger than 5 T. On the other hand, for the in-plane magnetic fields, the superconductivity is not completely suppressed, nor does it revert to the normal state even on applying a 55 T magnetic field at 1.5 K. We summarize both $H_{c2}^{\parallel}(T)$ and $H_{c2}^{\perp}(T)$ in Fig. 3c. We note that $H_{c2}^{\parallel}(T)$ increases with decreasing temperature and eventually saturates at approximately 52 T at 1.5 K, which is more than four times larger than $\mu_0 H_P^{BCS} = 12$ T. Because the orbital limit is supposed to be large owing to confinement of the geometry by the EDLT, the saturating behaviour of $H_{c2}^{\parallel}(T)$ at low temperatures is suggestive of the Pauli limit, as seen in the Pauli-limited superconductor[35].

The enhancement of H_{c2} in a dirty-limit superconductor with strong SOI has been discussed in terms of the spin–orbit scattering

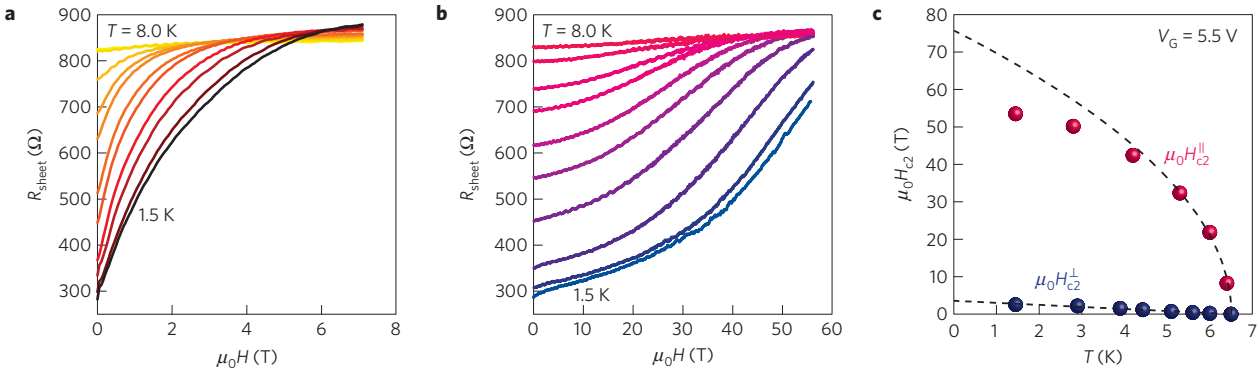

Figure 3 | Huge upper critical fields in ion-gated MoS_2. a,**b**, Sheet resistance of a MoS_2-EDLT at $V_G = 5.5$ V as a function of magnetic field up to 7 T for perpendicular magnetic fields $\mu_0 H^{\perp}$ at 1.5, 2.9, 3.9, 4.4, 5.1, 5.6, 6, 6.5, 6.8, 7.3 and 8.0 K (**a**) and up to 55 T for parallel magnetic fields $\mu_0 H^{\parallel}$ at 1.5, 2.8, 4.2, 5.3, 6, 6.4, 6.5, 6.8, 7.1, 7.6 and 8.0 K (**b**). **c**, In-plane and out-of-plane upper critical fields as a function of temperature. H_{c2} is defined as the magnetic field where R_{sheet} reached 75% of the normal state sheet resistance. The black dashed curves show the 2D-GL model. The value of $H_{c2}^{\parallel}$ increases with decreasing temperature, following the 2D-GL model near T_c, but deviates from the model at lower temperatures and eventually saturates at approximately 52 T at 1.5 K, suggestive of an enhancement of the Pauli limit.

caused by disorder. This is expected to cause randomization of electron spins, and thus result in suppression of the effect of spin paramagnetism[36–38]. To evaluate the contribution of this effect, we fitted our $H_{c2}^{\parallel}(T)$ data by using the microscopic Klemm–Luther–Beasely (KLB) theory[38], which is applicable to dirty-limit layered superconductors with strong SOIs ($l \ll \xi_{Pippard}$ and $\tau \ll \tau_{SO}$, where l, $\xi_{Pippard}$, τ and τ_{SO} are the mean free length, the Pippard coherence length, the total scattering time and the spin–orbit scattering time, respectively). Our $H_{c2}^{\parallel}(T)$ data are fitted well by the KLB theory (Supplementary Fig. 3); however, we found that in all cases the values of τ are larger than those of $\tau_{SO}(\tau > \tau_{SO})$ (Supplementary Table 1). This is an unphysical situation which contradicts with the initial assumption required for this theory ($\tau \ll \tau_{SO}$). Thus, the model with the effect of spin–orbit scattering does not explain the enhancement of $H_{c2}^{\parallel}$ consistently.

To find a more plausible origin of the enhancement of the Pauli limit in the present system, we first performed a set of *ab-intio*-based tight-binding supercell calculations on bulk MoS_2, incorporating the near-surface band bending effect via an electrostatic potential term obtained by self-consistently solving the Poisson equation (details in Supplementary Section IV). Our calculations suggest that, under the application of a strong electric field, a high-density 2DES is created at the surface of MoS_2. As schematically shown in Fig. 1d, this results in the formation of an accumulation layer, which is effectively confined within the topmost MoS_2 layer[39,40], indicating that non-centrosymmetric quasi-single-layer superconductivity is realized in our system. Such a "quasi-single-layer" 2DES, therefore, ought to have an effective D_{3h} symmetry, leading to many interesting features in the momentum space. For example, once a positive gate voltage is switched on, the conduction band minimum shifts to the ±K points[40]. This situation is in stark contrast to the case of bulk MoS_2, where the conduction band minima are located at six symmetrically equivalent k points along Γ–K directions, also known as the T (or Q) points[23,24]. Accordingly, the electric-field-induced 2D superconductivity in MoS_2 is expected to be solely mediated by the ±K valleys, and thus the most likely ground state of the Cooper pair should be the inter-valley pairing between the +K and −K valleys to maintain zero momentum for the centre-of-mass of the Cooper pairs. Note that the intra-valley spin-singlet Cooper pairs are not stabilized in the presence of the Zeeman-type SOI, which requires non-zero momentum.

At a sheet carrier density of $n_{2D} = 8.7 \times 10^{13}$ cm^{-2}, which is nearly the same as the value in the high-field measurement, the bands are spin-split by ∼3 meV at the ±K points, at zero magnetic field. Slightly away from the K point, these spin-split bands cross each other such that the splitting becomes ∼13 meV at the Fermi level. The corresponding band dispersion and spin texture at the Fermi surface are shown in Fig. 4a and b, respectively. All these features of the band structure are qualitatively equivalent to those in the monolayer MoS_2 derived from the tight-binding method[41] and the $k \cdot p$ model[42]. This agreement indicates that bulk or multilayer TMDs under a strong electric field can effectively behave as monolayers. Such a monolayer-like behaviour has already been experimentally demonstrated in bilayer systems, exhibiting circularly polarized photoluminescence under an electric field[43], and bulk systems showing gate-induced weak anti-localization behaviour in magnetoconductance[21]. In addition to these works, recent optical measurements on WSe_2 multilayers have shown that these systems can emit an electrically switchable circularly polarized electroluminescence[16]. The circularly polarized luminescence is believed to be a unique feature of the monolayer. Hence, the observation of the same phenomenon in a gated multilayer system provides strong evidence that TMDs such as MoS_2 can behave like a monolayer under an electric field.

As shown in Fig. 4a, each band is almost fully out-of-plane spin polarized. The in-plane Rashba-type component, which originates from the asymmetric potential along the c-axis produced by the strong electric field (∼ 50 MV cm^{-1}) (Fig. 1d), is calculated to be very small, with less than 2% of the total spin polarization. This is indeed expected by group theory, ruling that no in-plane component is allowed at the K points owing to their three-fold rotational (C_3) symmetry[44,45]. In the presence of the finite Rashba-type SOI, a Fulde–Ferrell–Larkin–Ovchinnikov (FFLO) state[4–6] (a helical state[46]), where Cooper pairs have non-zero momentum, with $s+f$-wave symmetry[47], is likely to be realized. However, we confirmed by a numerical calculation that the enhancement of the upper critical field due to the FFLO state, or induced spin-triplet components derived from Zeeman-type SOI, is negligible (see ref. 48 and Supplementary Fig. 6). Note that this FFLO state, where Cooper pairs have a finite centre of mass momentum which is much smaller than K, should be distinguished from the intra-valley pairing. Also, as other possibilities for the enhancement of H_{c2}, Rashba-type SOI (refs 1–3), quantum critical point[49] and modified electron g-factor[1,30] can be ruled out in the present system (details in Supplementary Section III). Therefore, spin–valley locking due to intrinsic Zeeman-type SOI is considered to be the most promising origin for the enhancement of $H_{c2}^{\parallel}$.

We theoretically estimated the realistic Pauli limit of the present system by considering both the Zeeman-type and the small Rashba-type SOIs. For this purpose, we constructed a simpler

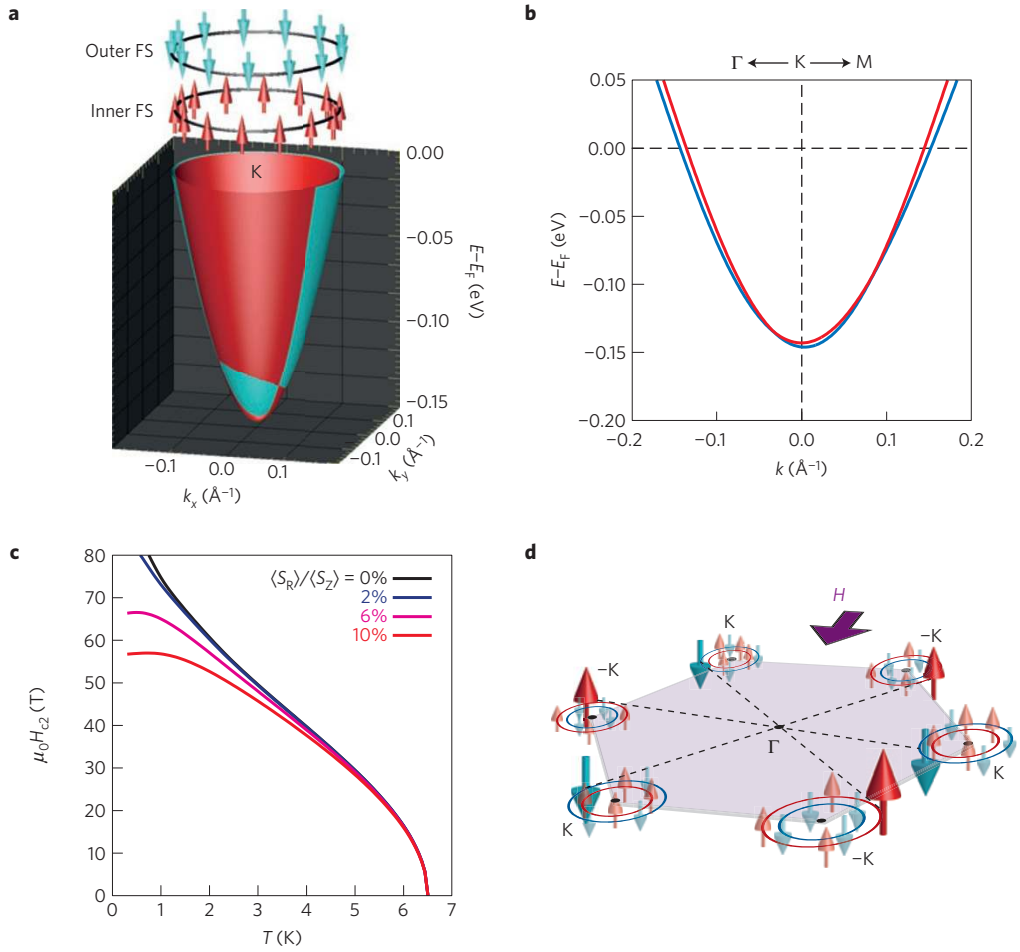

Figure 4 | Ising pairing protected by spin–valley locking in electric-field-induced 2D superconductivity in MoS_2. a, Energy band dispersion and spin texture of the conduction band around the K point of bulk MoS_2 under a strong electric field at $n_{2D} = 8.7 \times 10^{13}$ cm^{-2}. The inner Fermi surface (FS) and the outer FS at the K points have out-of-plane spin polarization with opposite directions because each band is almost fully out-of-plane spin polarized by the effective valley Zeeman fields, whereas the in-plane Rashba-type component is very small, with less than 2% of the total spin polarization. **b**, Two-dimensional energy band dispersion near the K point. The spin-split bands cross each other. The splitting at the Fermi level becomes ~13 meV, whereas that at the K point is ~3 meV. **c**, Theoretical curves of the Pauli limit considering both the Zeeman-type and small Rashba-type SOIs (see also Supplementary Figs 5 and 7). Black curve is the upper critical field in the tight-binding model reproducing the band structure calculation (Supplementary Fig. 4). The ratio of the Rashba-type and Zeeman-type SOIs, $\langle S_R \rangle / \langle S_Z \rangle$, is varied from 0 to 10%. **d**, Schematic image of the Fermi surfaces with valley-dependent spin polarization in the in-plane magnetic field geometry. The direction of each spin is orthogonal to the magnetic field. Inter-valley Ising pairing formed between the K and −K valleys is robust against an external magnetic field H, which realizes spin–valley-coupled 2D Ising superconductivity in ion-gated MoS_2.

tight-binding model reproducing the 2DES subband structure shown in Fig. 4b (see Supplementary Section IV and Supplementary Fig. 4). Assuming isotropic *s*-wave superconductivity, we then calculated the Pauli limit in this model by solving the linearized BCS gap equation using a diagrammatic technique based on the 2DES subband structure[50] (see Supplementary Section V). Figure 4c shows the theoretical curves of the Pauli limit in this system. Considering only the Zeeman-type SOI, the Pauli limit is considerably enhanced, as it is larger than 70 T at $T = 1$ K (see also Supplementary Fig. 5). This result indicates that the moderately large valley-dependent Zeeman-type spin splitting in the vicinity of the K points (~13 meV) protects singlet Cooper pairing between the K and −K valleys (Fig. 4d)—namely, the Cooper pairing locked by out-of-plane spin polarization to the two opposite directions, referred to as inter-valley Ising pairing, enhances $H_{c2}^{\parallel}$ much more than the H_P^{BCS}.

By contrast, once the small Rashba-type SOI is included, the enhanced Pauli limit is considerably suppressed, indicating that the symmetrical protection by spin–valley locking is weakened (Fig. 4c). This is because the in-plane polarized spin components due to the Rashba-type SOI are much more susceptible to an external in-plane magnetic field in comparison to the out-of-plane polarized spins due to the intrinsic Zeeman-type SOI. The best agreement with the experimental data is obtained for a moderate Rashba-type SOI of 10% of the Zeeman-type SOI, although such a Rashba-type SOI is unlikely according to the first-principles-based band calculations, as mentioned above. We discuss three possible origins for this discrepancy between the theoretical results based on a single-layer tight-binding model and the experimental results in Supplementary Section VI. In addition, according to our numerical calculations, which include the dependence on both the carrier density and T_c, the Pauli limit is predominantly controlled by both the Zeeman-type SOI and T_c, and the contribution of the Rashba-type SOI is negligibly small, in the range of carrier density where superconductivity is realized in this system (Supplementary Fig. 7). These results demonstrate that, by the application of a strong electric field, MoS_2, which is believed to be a conventional superconductor in the intercalated bulk form, becomes an unconventional 2D Ising superconductor in which Cooper pairs are protected by Zeeman-type spin–valley locking, and are thereby very robust against external magnetic fields, which

results in the marked enhancement of the Pauli limit. Our findings therefore indicate that, combined with highly crystalline materials, the exotic properties of superconductivity are now accessible through geometrical confinement using strong electric fields, which suggests that electric-field-induced superconductivity offers an ideal platform for unveiling the intrinsic nature of matter.

Note added in proof: We became aware of recent published similar experimental works on $NbSe_2$ (ref. 51) and ion-gated MoS_2 (ref. 52).

Methods

Methods and any associated references are available in the online version of the paper.

Received 15 June 2015; accepted 30 October 2015; published online 7 December 2015

References

1. Bauer, E. & Sigrist, M. *Non-Centrosymmetric Superconductors: Introduction and Overview* (Springer, 2012).
2. Yip, S. K. Two-dimensional superconductivity with strong spin–orbit interaction. *Phys. Rev. B* **65,** 144508 (2001).
3. Gor'kov, L. P. & Rashba, E. I. Superconducting 2D system with lifted spin degeneracy: Mixed singlet-triplet state. *Phys. Rev. Lett.* **87,** 037004 (2001).
4. Frigeri, P. A., Agterberg, D. F., Koga, A. & Sigrist, M. Superconductivity without inversion symmetry: MnSi versus $CePt_3Si$. *Phys. Rev. Lett.* **92,** 097001 (2004).
5. Fulde, P. & Ferrell, R. A. Superconductivity in a strong spin-exchange field. *Phys. Rev.* **135,** A550–A563 (1964).
6. Larkin, A. I. & Ovchinnikov, Y. N. Nonuniform state of superconductors. *Sov. Phys. JETP* **20,** 762–769 (1965).
7. Rashba, E. I. Properties of semiconductors with an extremum loop 1 cyclotron and combinational resonance in a magnetic field perpendicular to the plane of the loop. *Sov. Phys. Solid State* **2,** 1109–1122 (1960).
8. Zhu, Z. Y., Cheng, Y. C. & Schwingenschlogl, U. Giant spin–orbit-induced spin splitting in two-dimensional transition-metal dichalcogenide semiconductors. *Phys. Rev. B* **84,** 153402 (2011).
9. Xiao, D., Liu, G.-B., Feng, W., Xu, X. & Yao, W. Coupled spin and valley physics in monolayers of MoS_2 and other group-VI dichalcogenides. *Phys. Rev. Lett.* **108,** 196802 (2010).
10. Kormányos, A., Zólyomi, V., Drummond, N. D. & Burkard, G. Spin–orbit coupling, quantum dots, and qubits in monolayer transition metal dichalcogenides. *Phys. Rev. X* **4,** 011034 (2014).
11. Mak, K. F., Lee, C., Hone, J., Shan, J. & Heinz, T. F. Atomically thin MoS_2: A new direct gap semiconductor. *Phys. Rev. Lett.* **105,** 136805 (2010).
12. Wang, Q. H., Kalantar-Zadeh, K., Kis, A., Coleman, J. N. & Strano, M. S. Electronics and optoelectronics of two-dimensional transition metal dichalcogenides. *Nature Nanotech.* **7,** 699–712 (2012).
13. Wu, W. *et al.* Piezoelectricity of single-atomic-layer MoS_2 for energy conversion and piezotronics. *Nature* **514,** 470–474 (2014).
14. Sangwan, V. K. *et al.* Gate-tunable memristive phenomena mediated by grain boundaries in single-layer MoS_2. *Nature Nanotech.* **10,** 403–406 (2015).
15. Wu, S. *et al.* Monolayer semiconductor nanocavity lasers with ultralow thresholds. *Nature* **520,** 69–72 (2015).
16. Zhang, Y. J., Oka, T., Suzuki, R., Ye, J. T. & Iwasa, Y. Electrically switchable chiral light-emitting transistor. *Science* **344,** 725–728 (2014).
17. Mak, K. F., McGill, K. L., Park, J. & McEuen, P. L. The valley Hall effect in MoS_2transistors. *Science* **344,** 1489–1492 (2014).
18. Xu, X., Yao, W., Xiao, D. & Heinz, T. F. Spin and pseudospins in layered transition metal dichalcogenides. *Nature Phys.* **10,** 343–350 (2014).
19. Cui, X. *et al.* Multi-terminal transport measurements of molybdenum disulphide using van der Waals heterostructure device platform. *Nature Nanotech.* **10,** 534–540 (2015).
20. Ye, J. T. *et al.* Superconducting dome in a gate-tuned band insulator. *Science* **338,** 1193–1196 (2012).
21. Yuan, H. T. *et al.* Zeeman-type spin splitting controlled by an electric field. *Nature Phys.* **9,** 563–569 (2013).
22. Kormányos, A. *et al.* Trigonal warping, the Γ valley, and spin–orbit coupling effects. *Phys. Rev. B* **88,** 045416 (2013).
23. Coehoorn, R. *et al.* Electronic structure of $MoSe_2$, MoS_2, and WSe_2. I. Band-structure calculations and photoelectron spectroscopy. *Phys. Rev. B* **35,** 6195–6202 (1987).
24. Molina-Sánchez, A., Sangalli, D., Hummer, K., Marini, A. & Wirtz, L. Effect of spin–orbit interaction on the optical spectra of single-layer, double-layer, and bulk MoS_2. *Phys. Rev. B* **88,** 045412 (2013).
25. Ge, Y. & Liu, A. Y. Phonon-mediated superconductivity in electron-doped single-layer MoS_2: A first-principles prediction. *Phys. Rev. B* **87,** 241408(R) (2013).
26. Roldan, R., Cappelluti, E. & Guinea, F. Interactions and superconductivity in heavily doped MoS_2. *Phys. Rev. B* **88,** 054515 (2013).
27. Yuan, N. F. Q., Mak, K. F. & Law, K. T. Possible topological superconducting phases of MoS_2. *Phys. Rev. Lett.* **113,** 097001 (2014).
28. Rösner, M., Haas, S. & Wehling, T. O. Phase diagram of electron-doped dichalcogenides. *Phys. Rev. B* **90,** 245105 (2014).
29. Das, T. & Dolui, K. Superconducting dome in MoS_2 and $TiSe_2$ generated by quasiparticle-phonon coupling. *Phys. Rev. B* **91,** 094510 (2015).
30. Tinkham, M. *Introduction to Superconductivity* 2nd edn (Dover, 2004).
31. Reyren, N. *et al.* Superconducting interfaces between insulating oxides. *Science* **317,** 1196–1199 (2007).
32. Kim, M., Kozuka, Y., Bell, C., Hikita, Y. & Hwang, H. Y. Intrinsic spin–orbit coupling in superconducting δ-doped $SrTiO_3$ heterostructures. *Phys. Rev. B* **86,** 085121 (2012).
33. Ueno, K. *et al.* Effective thickness of two-dimensional superconductivity in a tunable triangular quantum well of $SrTiO_3$. *Phys. Rev. B* **89,** 020508(R) (2014).
34. Woolam, J. B. & Somoano, R. B. Physics and chemistry of MoS_2 intercalation compounds. *Mater. Sci. Eng.* **31,** 289–295 (1977).
35. Matsuda, Y. & Shimahara, H. Fulde–Ferrell–Larkin–Ovchinnikov superconductivity near the antiferromagnetic quantum critical point. *J. Phys. Soc. Jpn* **77,** 063705 (2008).
36. Maki, K. Effect of Pauli paramagnetism on magnetic properties of high-field superconductors. *Phys. Rev.* **148,** 362–369 (1966).
37. Werthamer, N. R., Helfand, E. & Hohenberg, P. C. Temperature and purity dependence of the superconducting critical field, H_{c2}. III. Electron spin and spin–orbit effects. *Phys. Rev.* **147,** 295–302 (1966).
38. Klemm, R. A., Luther, A. & Beasley, M. R. Theory of upper critical-field in layered superconductors. *Phys. Rev. B* **12,** 877–891 (1975).
39. Cuong, N. T., Otani, M. & Okada, S. Gate-induced electron-state tuning of MoS_2: First-principles calculations. *J. Phys. Condens. Matter* **26,** 135001 (2014).
40. Brumme, T., Calandra, M. & Mauri, F. First-principle theory of field-effect doping in transition-metal dichalcogenides: Structural properties, electronic structure, Hall coefficient, and electrical conductivity. *Phys. Rev. B* **91,** 155436 (2015).
41. Liu, G.-B., Shan, W.-Y., Yao, Y., Yao, W. & Xiao, D. Three-band tight-binding model for monolayers of group-VIB transition metal dichalcogenides. *Phys. Rev. B* **88,** 085433 (2013).
42. Kormányos, A. *et al.* $\mathbf{k}\cdot\mathbf{p}$ theory for two-dimensional transition metal dichalcogenide semiconductors. *2D Mater.* **2,** 022001 (2015).
43. Wu, S. *et al.* Electrical tuning of valley magnetic moment through symmetry control in bilayer MoS_2. *Nature Phys.* **9,** 149–153 (2013).
44. Dresslhaus, M. S., Dresselhaus, G. & Jorio, A. *Group Theory: Application to the Physics of Condensed Matter* (Springer, 2008).
45. Oguchi, T. & Shishidou, T. The surface Rashba effect: A $\mathbf{k}\cdot\mathbf{p}$ perturbation approach. *J. Phys. Condens. Matter* **21,** 092001 (2009).
46. Kaur, R. P., Agterberg, D. F. & Sigrist, M. Helical vortex phase in the noncentrosymmetric $CePt_3Si$. *Phys. Rev. Lett.* **94,** 137002 (2005).
47. Frigeri, P. A. *Superconductivity in Crystals Without an Inversion Center* PhD thesis, ETH Zurich (2005).
48. Yanase, Y. & Sigrist, M. Magnetic properties in non-centrosymmetric superconductors with and without antiferromagnetic order. *J. Phys. Soc. Jpn* **76,** 124709 (2007).
49. Tada, Y., Kawakami, N. & Fujimoto, S. Colossal enhancement of upper critical fields in noncentrosymmetric heavy fermion superconductors near quantum criticality: $CeRhSi_3$ and $CeIrSi_3$. *Phys. Rev. Lett.* **101,** 267006 (2008).
50. Nakamura, Y. & Yanase, Y. Multi-orbital superconductivity in $SrTiO_3/LaAlO_3$ interface and $SrTiO_3$ surface. *J. Phys. Soc. Jpn* **82,** 083705 (2013).
51. Xi, X *et al.* Ising pairing in superconducting $NbSe_2$ atomic layers. *Nature Phys.* http://dx.doi.org/10.1038/nphys3538 (2015).
52. Lu, J. M. *et al.* Evidence for two-dimensional Ising superconductivity in gated MoS_2. *Science* http://dx.doi.org/10.1126/science.aab2277 (2015).

Acknowledgements

We thank T. Gokuden for technical support, and M. Yoshida and K. Kikutake for fruitful discussions. Y.S. and Y. Nakamura were supported by the Japan Society for the Promotion of Science (JSPS) through a Research Fellowship for Young Scientists. This work was supported by Grant-in-Aid for Specially Promoted Research (no. 25000003) from JSPS and Grant-in Aid for Scientific Research on Innovative Areas (no. 22103004) from MEXT of Japan.

Author contributions

Y.S. and Y.I. conceived the idea and designed the experiments. Y.S., Y. Nakagawa and M.O. fabricated MoS_2-EDLT devices. Y.S. conducted cryogenic transport measurements

with the PPMS set-up, and analysed the data. M.S.B. carried out *ab initio*-based tight-binding supercell calculations. Y. Nakamura performed numerical calculations of the upper critical field. Y.S., Y. Kasahara and Y. Kohama carried out high-field measurements in the Institute for Solid State Physics. J.Y. took leadership of the initial high-field experiment when he was in the University of Tokyo and RIKEN. M.T., Y. Kasahara and T.N. led physical discussions. Y.S., M.S.B., T.N., Y.Y. and Y.I. wrote the manuscript.

Additional information

Supplementary information is available in the online version of the paper. Reprints and permissions information is available online at www.nature.com/reprints. Correspondence and requests for materials should be addressed to Y.S. or Y.I.

Competing financial interests

The authors declare no competing financial interests.

Methods

Device fabrication. Bulk 2*H*-polytype MoS_2 single crystals were cleaved into thin flakes with tens of nanometres in thickness using the Scotch-tape method. The flakes were then transferred onto Si/SiO_2 substrates or Nb-doped $SrTiO_3/HfO_2$ substrates. Au (90 nm)/Cr (5 nm) electrodes were patterned onto an isolated thin flake in a Hall bar configuration, and a side gate electrode was patterned onto the substrate. We covered the device with ZEP 520A (used as the resist for electron beam lithography), except for the channel surface, to avoid chemical intercalation from the edge of the flake, allowing us to focus on the field effect. A droplet of ionic liquid covered both the channel area and the gate electrode. The ionic liquid N,N-diethyl-N-(2-methoxyethyl)-N-methylammonium bis (trifluoromethylsulphonyl) imide (DEME-TFSI) was selected as a gate medium.

Transport measurements. The temperature-dependent resistance, under magnetic fields, of the MoS_2-EDLT (shown in Fig. 2) was measured with a standard four-probe geometry in a Quantum Design Physical Property Measurement System (PPMS) with a Horizontal Rotator Probe with an error below 0.01°, combined with two kinds of a.c. lock-in amplifier (Stanford Research Systems Model SR830 DSP lock-in amplifier and Signal Recovery Model 5210 lock-in amplifier). The gate voltage was supplied by a Keithley 2400 sourcemeter. We applied gate voltages to the device at 220 K, which is just above the glass transition temperature of DEME-TFSI, under high vacuum (less than 10^{-4} torr), and cooled down to low temperatures. The excitation source–drain current used in the PPMS set-up was limited to 1 μA to avoid heating and large-current effects on the superconductivity.